Biochemistry

 Volume 34, Number 26 July 4, 1995

Accelerated Publications

Cryo Atomic Force Microscopy: A New Approach for Biological Imaging at High Resolution†

Wenhai Han, Jianxun Mou, Jun Sheng, Jie Yang,‡ and Zhifeng Shao*

Department of Molecular Physiology and Biological Physics and Biophysics Program, University of Virginia School of Medicine, Box 449, Charlottesville, Virginia 22908

Received May 2, 1995®

ABSTRACT: A low-temperature atomic force microscope (cryo-AFM), operated in liquid nitrogen vapor, has been constructed for biological applications. The system provides an adjustable imaging temperature from 77 to 220 K with atomic resolution achieved on crystalline specimens. Imaging with NaCl microcrystals demonstrates that the system is free from surface contamination. Below 100 K, several biological specimens, including immunoglobulins and DNA as well as red blood cell ghosts, were imaged at high spatial resolution. Measurements on individual macromolecules showed that the mechanical strength is significantly greater at cryogenic temperatures with an estimated Young's modulus 1000−10 000 times that of a hydrated protein at room temperature, providing a solid basis for future improvements and applications of cryo-AFM in structural biology.

Although atomic force microscopy (AFM) (Binnig et al., 1986; Alexander et al., 1989) has been applied to various biological specimens with encouraging successes as documented by many recent reviews (Hansma & Hoh, 1994; Bustamante et al., 1994; Yang & Shao, 1995; Shao & Yang, 1995), nanometer resolution was only achieved in several cases, such as bacterial toxins (Yang et al., 1993b, 1994b), bacterial outer membrane proteins (Karrasch et al., 1994; Schabert & Engel, 1994; Schabert et al., 1995), and gap junctions (Hoh et al., 1991), either in closely packed specimens or in two-dimensional crystals. In most other cases, the resolution has been at least an order of magnitude lower (Yang et al., 1994a; Braunstein & Spudich, 1994; Henderson et al., 1992). For very flexible macromolecules, the AFM so far has failed to yield useful images of recognizable structures (Ill et al., 1993; Yang et al., 1994a). The difficulty in achieving high resolution on hydrated proteins has been attributed, among other factors (Bustamante et al., 1994), to the deformation or damage induced by the probe force, due to the very high pressure in the contact area even at sub-nano-Newton forces and the softness of most hydrated biological specimens (Shao & Yang, 1995). It has been suggested that imaging biological samples at cryogenic temperatures could overcome many of these limitations (Prater et al., 1991; Yang et al., 1993a; Shattuck et al., 1994) on the basis of macroscopic measurements of biological samples (Dorrington, 1979) and studies of enzyme activities (Perutz, 1992) at cryogenic temperatures. However, the elastic property at the molecular scale cannot be directly inferred from these experiments, as this requires direct measurements on individual macromolecules under various compression forces. To perform such experiments, a high-performance cryo-AFM[1] is the necessary first step.

To date, very few attempts have been made to construct a reliable cryo-AFM for the purpose of biological imaging

† This work is supported by grants from the National Institutes of Health (RO1-RR07720 and PO1-HL48807) and the National Science Foundation (BIR-9195655).

* To whom correspondence should be addressed.

‡ Present address: Department of Physics, University of Vermont, Burlington, VT 05405.

0006-2960/95/0434-8215$09.00/0

(Prater et al., 1991; Mou et al., 1993; Shattuck et al., 1994). The main difficulty is the protection of the specimen surface from adsorbing contaminants (Prater et al., 1991; Mou et al., 1993), which not only cover up the structures to be imaged but also contaminate AFM tips themselves, resulting in unacceptably large adhesion forces and poor resolution (Prater et al., 1991; Yang & Shao, 1993). Since frozen biological samples contain large amounts of vitrified ice and are damaged at high baking temperatures, a vacuum-based cryo-AFM has been shown inadequate (Prater et al., 1991) where surface contamination was found extensive. To overcome these problems, we have introduced a novel concept (Mou et al., 1993) that the cryo-AFM is operated in a cryogenic gas under ambient pressure.

In this paper, we report the performance of a cryo-AFM operated in liquid nitrogen (LN_2) vapor. With this novel instrument, surface contamination is entirely eliminated and several biological specimens have been successfully imaged, using commercial AFM cantilevers, with excellent reproducibility and a much improved resolution compared with room temperature AFM on similar specimens. The resolution demonstrated already succeeded that of scanning electron microscopy and is comparable to that of conventional transmission electron microscopy. Direct measurements on individual macromolecules indicate that the Young's modulus at cryogenic temperatures is at least several thousand times that at room temperature, which suggests that, with a super sharp tip (Keller & Chi-Chung, 1992), the spatial resolution can be further improved.

MATERIALS AND METHODS

Instrumentation. The cryo-AFM is housed in a custom-built superinsulated dewar (Precision Cryogenics, Indianapolis, IN), where the inside pressure is maintained to slightly above the ambient pressure via two relieve valves. The system is illustrated in Figure 1A, and the functions of various parts are explained in the figure legend. Normally, 100−150 L of LN_2 is stored in the dewar to maintain temperature stability in the AFM. Optical detection of the cantilever deflection is used in this design where both the laser diode and the photodiode detector are operated at cryogenic temperatures. Laser alignment and all other operations are performed from the outside, but the AFM is suspended on four springs combined with magnetic damping. During imaging, all adjustments are disconnected to ensure sufficient mechanical stability. Both the specimen and the cantilever can be replaced *in situ* without raising the temperature of the system, so that a contamination-free imaging environment can be attained indefinitely. The stable temperature gradient in the dewar can be used for AFM imaging at various temperatures between 77 and 220 K by placing the AFM at different positions in the dewar. Cantilevers used were custom ordered from Park Scientific (Sunnyvale, CA) without any metal coating, because the differential shrinkage of the materials caused excessive bending of the cantilever, such that the laser beam could not be aligned. All the images presented in this paper were obtained with cantilevers of a nominal room temperature spring constant 0.03 N/m. At around 100 K, the spring

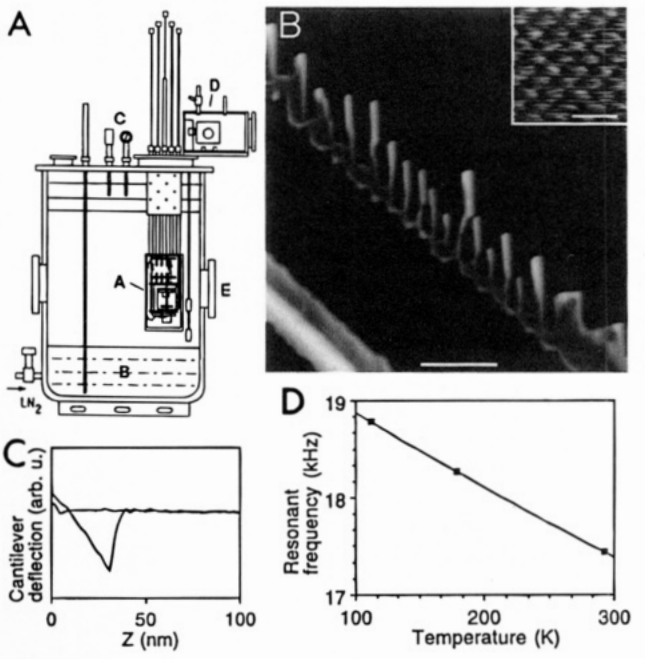

FIGURE 1: (A) Illustration of the cryo-AFM system operated in LN_2 vapor. Optical detection is used to monitor the cantilever deflection. Both the laser diode and the photodiode are operated at cryogenic temperatures. The specimen and the cantilever can be exchanged *in situ*, so the AFM (A) can remain at cryogenic temperatures all the time to maintain a clean imaging environment. The chamber for specimen preparation and sample/tip exchange is seen at the top of the dewar (D). All mechanical controls and adjustments are disengaged during imaging. LN_2 at the bottom (B) serves as a huge cold trap. Inside pressure is regulated by relief valves (C) to a few psi above the atmospheric pressure. (B) An image of NaCl microcrystals obtained at 96 K at a line scan speed of 2 Hz. The specimen was prepared by precipitating a small droplet of 20 mM NaCl solution on a freshly cleaved mica surface under nitrogen. The smallest width of these microcrystals is only about 80 nm wide. Scale bar: 1 μm. (Inset) High-resolution image obtained on these microcrystals, showing the well-resolved cubic lattice of the (100) surface (0.4 nm) (original data without processing). Scale bar: 1 nm. AFM at room temperature in air did not yield useful images on similar specimens, due to unstable adhesion to the substrate. (C) Force vs distance curve obtained at 88 K, which can be maintained over long periods of time. The adhesion force is less than 1 nN, indicating a clean and stable specimen surface. (D) Shift of one of the resonant frequencies vs temperature.

constant is about 15% greater (~0.035 N/m), according to the shift in the resonant frequencies. The line scan speed was 1−2 Hz with 512 pixels per line. All scales were calibrated against a gold-coated grating of known dimensions at the imaging temperature and rechecked with mica and graphite. The piezo sensitivity remained stable over many temperature cycles. The cryo-AFM is interfaced to NanoScope III AFM control electronics (Digital Instruments, Santa Barbara, CA).

Materials. Plasmid DNA (5.2 kb), immunoglobulins G (IgG) and M (IgM), obtained from Sigma Chemicals (St. Louis, MO), were used without further purification. Right before use, the stock solution (1 mg/mL) was further diluted to a concentration of 1−2 μg/mL in the appropriate buffer. Red blood cell ghosts were prepared according to the well-established procedures (Yu et al., 1973; Steck & Kant, 1974). Briefly, freshly drawn rabbit blood was first washed in PBS with centrifugation at 1000*g*. The pelleted cells were resuspended in diluted PBS (1:100) at pH 7.4 with a volume ratio of 1:15. After repeated centrifugation at 20000*g* for

[1] Abbreviations: cryo-AFM, cryo atomic force microscope; LN_2, liquid nitrogen; IgG, immunoglobulin G; IgM, immunoglobulin M; PBS, phosphate-buffered saline.

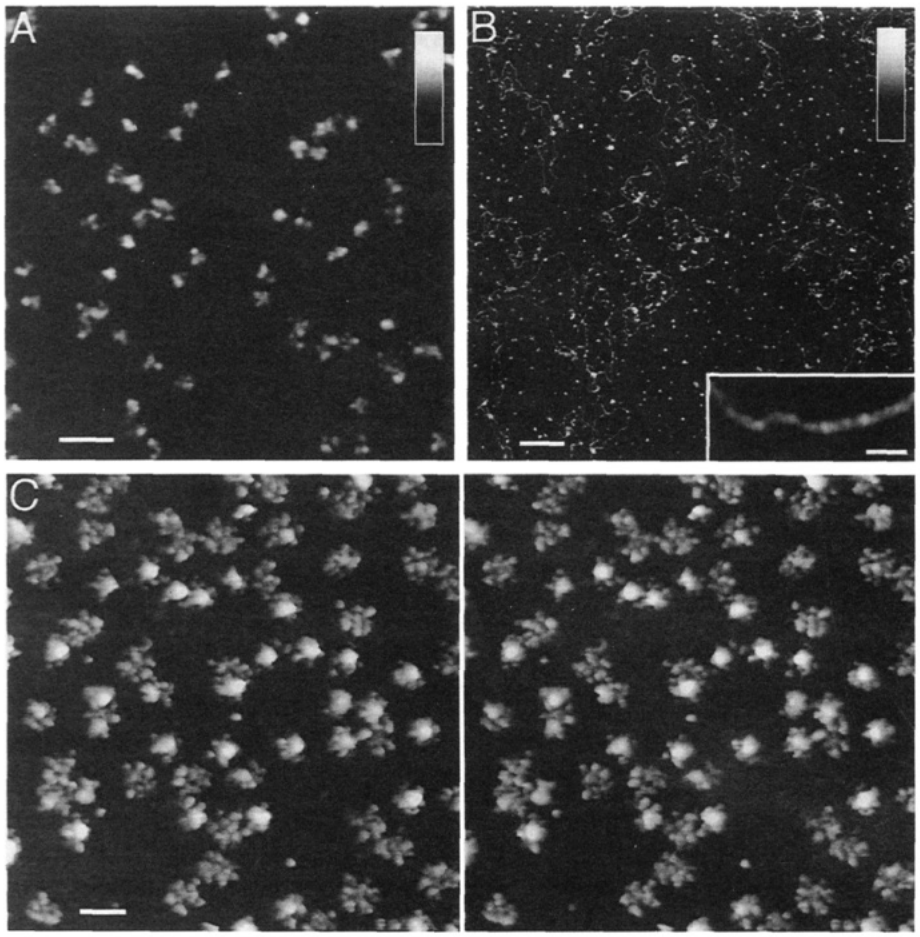

FIGURE 2: AFM images of several macromolecules obtained at temperatures below 100 K. All images are original data without processing, except for the inset in panel B where a low-pass filter was used. (A) IgG molecules at 89 K. The characteristic Y-shape can be identified on many molecules, as well as other conformatioins and orientations, along with some large aggregates. The height measured from individual Y-shaped molecules is about 3 nm. Scale bar: 50 nm. Height bar: 7.5 nm. (B) Plasmid DNA (5.2 kb) at 95 K. Scale bar: 200 nm. Height bar: 2.5 nm. (Inset) Higher resolution image showing the ~3 nm modulation seen on some DNA molecules (constant height mode). But the pitch of the double helix is not consistently resolved, perhaps due to the salt deposited on the DNA which covered up the finer details. Scale bar: 10 nm. The height measured is about 1.2−1.5 nm. (C) A stereogram of IgM obtained at 87 K. This stereo pair is created by using the surface plot with two different viewing angles of 18° apart. The complicated molecular structure of this large flexible molecule of 21 polypeptides can only be appreciated in the stereogram. The two dominant conformations are recognizable (see text). Scale bar: 50 nm. The apparent height in the stereogram is slightly increased to show details.

40 min in diluted PBS, the pelleted red cell ghosts were resuspended in diluted PBS to the original volume. All these procedures were performed at 4 °C.

Specimen Preparation. All specimens were prepared with the following procedure: a droplet of solution, containing protein or DNA or red cell ghosts in an appropriate buffer, was applied to a freshly cleaved mica surface. After a short incubation, the specimen was washed extensively, and the excess solution was removed before it was transferred into the cryo-AFM already at the imaging (cryogenic) temperature. No other specimen treatment was needed or applied. All these procedures were operated under dry nitrogen to avoid contamination.

RESULTS AND DISCUSSION

Instrument Performance. There are several major advantages for AFM imaging in a cryogenic gas (LN_2 vapor), compared with other approaches (Prate et al., 1991; Giessibl & Binnig, 1992; Shattuck et al., 1994). Since the lowest temperature is at the bottom of the dewar where standing LN_2 exists all the time, it serves as an enormous cold trap absorbing most contaminants. A very clean imaging environment can thus be attained after a short settling time. In fact, the environment is continuously improved over time, because adsorbents are slowly transferred from higher temperature surfaces to lower temperature ones. It may be noted that, at temperatures around 100 K, the water pressure is already lower than 10^{-15} torr, better than any vacuum system can deliver (Anderson, 1989).[2] Compared with other approaches, this is perhaps the most important advantage of this approach. Secondly, vibrations due to LN_2 bubbling can be completely eliminated for more than 10 h by slightly increasing the inside pressure of the dewar to 5 psi, due to a slight shift of the boiling temperature and the large heat capacity of the system (up to 320 L of LN_2). Mechanical and acoustical coupling through LN_2 vapor is minimal, which is a prerequisite for achieving atomic resolution. Thirdly, the imaging temperature can be changed by simply changing the position of the AFM in respect to the stable temperature gradient in the dewar (from 77 to about 220 K). With the

[2] Note: In this reference, the vapor pressure of water is given only to 113 K. We extrapolated to 100 K according to the listed data and found that the pressure−temperature relationship follows the Clausius−Clapeyron law.

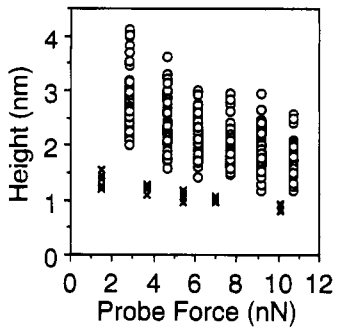

FIGURE 3: Molecular compression under various probe forces. Those from IgG are plotted with open circles and those from DNA with crosses. Imaging temperature was 89 K for IgG and 95 K for DNA. The larger variation of IgG measurements reflects different orientations of IgG molecules on the substrate. Within this force range, no plastic deformation was observed. It is interesting that, at small probe forces, IgG is much more compressible than DNA, but at large probe forces, the two are equivalent. These data represent the first such measurements on biological macromolecules at these temperatures, providing a solid basis for the relevance of cryo-AFM in biological applications.

superinsulated dewar, the temperature stability achieved at temperatures between 77 and 170 K was better than 4 mK/min, another prerequisite for achieving high resolution. Such a high stability is rather exceptional and enables the use of very slow scan speeds for improved signal to noise ratio. These principles are clearly demonstrated when crystalline specimens were imaged at atomic resolution. In Figure 1B, an image of precipitated NaCl microcrystals on a mica surface obtained by the cryo-AFM at 96 K is shown. On these crystals, the cubic lattice of the (100) surface (lattice spacing: 0.4 nm) is well resolved (Figure 1b inset), demonstrating the excellent mechanical and thermal stability of the system, since a very slow scan rate (2 lines per s at 512 pixels per line) was used. More importantly, the same resolution on the same specimen was achieved after more than a week of storage in the cryo-AFM without additional protection. This result firmly established that this cryo-AFM system is free from surface contamination, the most critical requirement for any cryo-AFM. A typical force curve is shown in Figure 1C, which can be maintained over long periods of time. Since the spring constant of the cantilever is about 0.035 N/m, the force curve shown in Figure 1C represents an adhesion force of below 1 nN, another indicator of a clean and stable specimen surface (Yang & Shao, 1993; Lyubchenko et al., 1992). Similar specimens did not yield useful images in air at room temperature due to unstable adhesion to the substrate.

Imaging of Purified Macromolecules. To establish the validity of the cryo-AFM and to characterize its performance, several biological macromolecules have been imaged in this system. In Figure 2A, an image of IgG obtained at 89 K is shown. The characteristic Y-shape is well resolved on many individual molecules, although other orientations and conformations can also be identified, which is perhaps the result of the extreme structural flexibility of this large molecule (~150 kDa). On those molecules with a symmetric Y-shape, the IgG measures about 12 nm on each side, consistent with electron microscopy (Green, 1969; Ryazantsev et al., 1989) and X-ray diffraction (Silverton et al., 1977; Davies & Metzger, 1983; Davies et al., 1975). Figure 2B shows another example: 5.2 kb plasmid DNA at 95 K. The full width at half-height measured from cross-sectional profiles is about 3 nm, with some measurements down to 2.6 nm. If this broadening is attributed to the finite tip size, 5 nm would be expected for the radius of curvature at the apex of the tip (Bustamante et al., 1994). However, it has been reported that interstrand spacing of DNA in a thin crystal could be up to 2.7 nm by electron diffraction (Downing, 1984). Therefore, it is also possible that bound salt and other adsorbents are responsible for the increased width of DNA. These two possibilities cannot be differentiated at present. Although ~3 nm modulations are discernible on some DNA molecules (see inset of Figure 2B), the pitch of the double helix was not convincingly resolved. The height directly measured for both IgG and DNA was somewhat lower, but no more than 1 nm, than the known values. Further investigation revealed that this reduced height was not due to probe-induced compression, since a thin solid layer of ~1 nm thick could always be scraped away by a stronger cantilever on the sample surface. Taking into account this adsorbent layer, the measured height would be consistent with the known values from other techniques. With the confirmative results of IgG and DNA, we further imaged a much more complex macromolecule, IgM (Parkhouse et al., 1970), at 87 K. To better convey the three-dimensional surface structure, a stereo representation is shown in Figure 2C. The five IgG subunits with a variable and complicated spatial arrangement are clearly resolved in the stereogram. The overall dimension varies from about 30 to 42 nm, generally consistent with the structure obtained by negatively stained electron microscopy (Parkhouse et al., 1970). On some of the molecules with a more extended appearance, the small central J-chain is also resolved. Among the two dominant conformations, the more compact form with a smaller lateral dimension and a much higher central core (4−5 nm) appeared more consistent with the constraints imposed by the disulfide bonds in IgM (Koshland, 1985). These images of IgG and IgM represent a significant improvement over those obtained by AFM at room temperatures, where the characteristic shapes of these molecules were never resolved even when stable adhesion was achieved (Weisenhorn et al., 1990; Ill et al., 1993; Yang et al., 1994a), due to their extreme flexibility, their weak adhesion to the substrate, and their "sticky" surface that adhered to the AFM tip readily. One common feature of all these specimens is their superior stability, which can withstand repeated scans at very slow scan rates, without damage or movement. The useful lifetime of a tip was also extended to many days, compared with hours at room temperature. The same resolution was obtained after days of storage in the cryo-AFM. Since all the images were obtained with commercial cantilevers without preselection or treatment (Keller & Chi-Chung, 1992), it appears that the resolution achieved so far is tip size limited. Therefore, sharper tips may significantly improve upon the resolution, because the improved mechanical strength of the macromolecules should be able to sustain a much higher probe pressure before any significant deformation or damage can occur (Shao & Yang, 1995).

Molecular Elasticity at Cryogenic Temperatures. Since one of the most important justifications for biological cryo-AFM is the improved mechanical strength of macromolecules, we have measured the amount of compression under various applied probe forces on individual macromolecules at cryogenic temperatures, so that the elastic properties can be determined at the molecular scale. The results for IgG

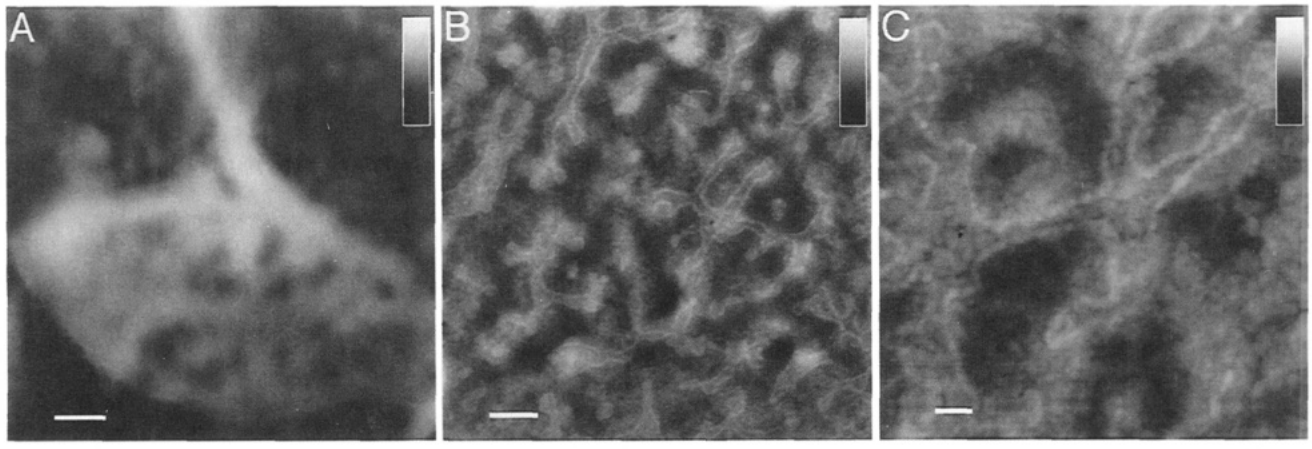

FIGURE 4: Cryo-AFM of red blood cell ghosts. (A) Part of an unsealed ghost. Notice the membrane folds in the image. The unsealed ghost is seen collapsed on the mica surface. Scale bar: 0.4 μm. Height bar: 100 nm. (B) At a higher resolution, intricate surface structures can be seen among large-scale surface corrugations. These line-type structures have a nominal width of 6−8 nm. Scale bar: 0.2 μm. Height bar: 20 nm. (C) At an even higher resolution, the line-type structure is resolved as individual particles of 6−8 nm along the lines, among similarly sized particles randomly distributed on the membrane surface. The smallest resolvable feature is about 4 nm, at least an order of magnitude better than that at room temperature. It is interesting that these molecules lined up to form complicated closed boundaries. Scale bar: 50 nm. Height bar: 20 nm.

at 89 K (open circles) and DNA at 95 K (crosses) are plotted in Figure 3. For IgG, the elastic response is nonlinear, with a spring constant of about 3 N/m at low-probe forces and about 17 N/m at high-probe forces. At 1 nN probe force, the compression is only about 3 Å, a significant improvement over that at room temperature (Yang et al., 1994a). Interestingly, for DNA, the elastic response appeared rather linear with a spring constant of about 17 N/m, reflecting the much higher stability due to base pairing. These data represent the first such measurements on individual macromolecules, consistent with a previous indirect measurement (Perutz, 1992). To calculate Young's modulus, the exact area of compression must be known, which cannot be determined precisely at present. However, if we assume a 10 nm^2 contact area as an upper limit, the lower limit of Young's modulus can be estimated as 10 500 kg/cm^2 for IgG and 20 700 kg/cm^2 for DNA at about 1 nN probe force, which is many orders of magnitude greater than that at room temperature, where Young's modulus could be as low as 5 kg/cm^2 for hydrated proteins (Morozov & Morozov, 1994; Urry, 1988). Specimen damage was not observed for probe forces up to 15 nN. The same structure at a similar resolution was always obtained as soon as the probe force was reduced to 1−2 nN. These observations also indicate that molecular damage caused by the tip is also greatly reduced at cryogenic temperatures.

Imaging Red Blood Cell Surface. Since the ability to image cell surfaces at high resolution has many important applications, such as determining membrane protein density (Quinn et al., 1984) and mapping receptor distributions (Metzger, 1992), we have applied the cryo-AFM to the imaging of unsealed red blood cell ghosts at 89 K (Figure 4). At a large scale (Figure 4A), membrane folds and the edge of a ghost can be seen. On the surface of the cell membrane, 5−10 nm molecules were seen almost everywhere (Figure 4C), which is a resolution of at least an order of magnitude higher than that at room temperature (Henderson et al., 1992; Shoenenberger & Hoh, 1994). The high protein density revealed in these images seems to provide a direct confirmation of a previous finding based on indirect measurements (Quinn et al., 1984). Most interestingly, some of these molecules are clearly seen forming closed boundaries (Figure 4B,C), a phenomenon previously not observed. It will be interesting if these membrane proteins can be identified with specific antibodies in future experiments. This example demonstrates the ability of cryo-AFM to image large biological structures with a minimal preparation at high spatial resolution.

In summary, we have established the relevance of a LN_2 vapor based cryo-AFM for biological imaging. Surface contamination is shown nearly nonexistent, and both mechanical and thermal stability is excellent, as demonstrated by the atomic resolution images of crystalline specimens. The increased mechanical strength measured from individual macromolecules provided a solid foundation for further improvement of spatial resolution to the subnanometer range with specially fabricated super sharp tips (Keller & Chi-Chung, 1992; Bustamante et al., 1994). In addition, the cryo-AFM also makes other applications possible. For example, the transmembrane domains of an integral membrane protein can be directly imaged with freeze fracture, providing information that is difficult to obtain with other techniques (Kühlbrandt, 1992). Sectional imaging may be achieved with a sequential imaging and removal of exposed structures following a controlled etching, which can be used to obtain 3-D structures of cells or nuclei, such as the chromosome structure in an intact nucleus under various conditions, avoiding possible artifacts associated with the purification of these very large, yet delicate molecular assemblies (van Holde, 1989). The realization of these imaging abilities with further development will make the cryo-AFM a powerful structural probe with its own unique advantages. Furthermore, this type of AFM is not limited to biological applications. It can also be used in materials research on those samples that are pressure and/or temperature sensitive.

ACKNOWLEDGMENT

We thank D. Czajkowsky for helpful discussions and Mr. Gang Huang for technical assistance. We also thank Drs. A. P. Somlyo and A. V. Somlyo for encouragement.

REFERENCES

Alexander, S., Hellemans, L., Marti, O., Schneir, J., Elings, V., & Hansma, P. (1989) *J. Appl. Phys. 65*, 164−167.

Anderson, H. L., Ed. (1989) *A Physicist's Desk Reference*, p 126, American Institute of Physics, New York.
Binnig, G., Quate, C., & Gerber, Ch. (1986) *Phys. Rev. Lett. 56*, 930−933.
Braunstein, D., & Spudich, A. (1994) *Biophys. J. 66*, 1717−1725.
Bustamante, C., Vesenka, J., Tang, C., Rees, W., Guthod, M., & Keller, R. (1992) *Biochemistry 31*, 22−26.
Bustamante, C., Erie, D., & Keller, D. (1994) *Curr. Opin. Struct. Biol. 4*, 750−760.
Davies, D., & Metzger, H. (1983) *Annu. Rev. Immunol. 1*, 87−117.
Davies, D., Padlan, E., & Segel, D. (1975) *Annu. Rev. Biochem. 44*, 639−667.
Dorrington, K. (1979) in *The Mechanical Properties of Biological Materials*, Cambridge University Press, Cambridge.
Downing, K. (1984) *Ultramicroscopy 13*, 35−46.
Giessibl, F., & Binnig, G. (1992) *Ultramicroscopy 42/44*, 281−289.
Green, N. M. (1969) *Adv. Immunol. 11*, 1−30.
Hansma, H., & Hoh, J. (1994) *Annu. Rev. Biophys. Biomol. Struct. 23*, 115−118.
Hansma, H., Browne, K., Bezanilla, H., & Bruice, T. (1994) *Biochemistry 33*, 8436−8441.
Henderson, E., Hayelon, P., & Sakaguchi, D. (1992) *Science 257*, 1944−1946.
Hoh, J., Lal, R., John, S., Revel, J., & Arnsdorf, M. (1991) *Science 253*, 1405−1408.
Ill, C., Keivens, V., Hale, J., Nakamura, K., Jue, R., Cheng, S., Melcher, E., Drake, B., & Smith, M. (1993) *Biophys. J. 64*, 919−924.
Karrasch, S., Hegerl, R., Hoh, J., Baumeister, W., & Engel, A. (1994) *Proc. Natl. Acad. Sci. U.S.A. 91*, 836−838.
Keller, D., & Chi-Chung, C. (1992) *Surface Sci. 268*, 333−339.
Koshland, M. E. (1985) *Annu. Rev. Immunol. 3*, 425−453.
Kühlbrandt, W. (1992) *Q. Rev. Biophys. 25*, 1−49.
Lyubchenko, Y., Jacobs, B., & Lindsay, S. (1992) *Nucleic Acids Res. 20*, 3983−3986.
Metzger, H. (1992) *J. Immunol. 149*, 1477−1487.
Morozov, V., & Morozov, T. (1994) *J. Biomol. Struct. Dyn. 11*, 459−481.
Mou, J., Yang, J., & Shao, Z. (1993) *Rev. Sci. Instrum. 64*, 1483−1488.
Parkhouse, R., Askonas, B., & Dourmashkin, R. (1970) *Immunology 18*, 575−584.
Perutz, M. (1992) *Nature 358*, 548.
Prater, C., Wilson, M., Carnaes, J., Massie, J., Elings, V., & Hansma, P. (1991) *J. Vac. Sci. Technol. B9*, 989−991.
Quinn, P., Griffiths, G., & Warren, G. (1984) *J. Cell. Biol. 98*, 2142−2147.
Rees, W., Keller, R., Vesenka, J., Yang, G., & Bustamante, C. (1993) *Science 260*, 1646−1649.
Ryazantsev, S. N., Vasiliev, V. D., Abramov, V. M., Franek, F., & Zav'yalov, V. P. (1989) *FEBS Lett. 244*, 291−295.
Schabert, F., & Engel, A. (1994) *Biophys. J. 67*, 2394−2403.
Schabert, F. A., Henn, C., & Engel, A. (1995) *Science 268*, 92−94.
Shao, Z., & Yang, J. (1995) *Q. Rev. Biophys.* (in press).
Shattuck, M., Gustafsson, M., Fisher, K., Yanagimoto, K., Veis, A., Bhatnagar, R., & Clarke, J. (1994) *J. Microsc. 174*, RP1−RP2.
Shoenenberger, C., & Hoh, J. (1994) *Biophys. J. 67*, 929−936.
Silverton, E., Navia, M., & Davies, D. (1977) *Proc. Natl. Acad. Sci. U.S.A. 74*, 5140−5144.
Steck, T., & Kant, J. (1974) *Methods Enzymol. 31*, 172−180.
Urry, D. (1988) *J. Protein Chem. 7*, 1−34.
van Holde, K. (1989) *Chromatin*, Springer-Verlag, New York.
Weisenhorn, A., Drake, B., Prater, C., Gould, S., Hansma, P., Ohnesorge, F., Egger, M., Heyn, S., & Gaub, H. (1990) *Biophys. J. 58*, 1251−1258.
Yang, J., & Shao, Z. (1993) *Ultramicroscopy 50*, 157−170.
Yang, J., & Shao, Z. (1995) *Micron 26*, 35−49.
Yang, J., Takeyasu, K., & Shao, Z. (1992) *FEBS Lett. 301*, 173−176.
Yang, J., Tamm, L., Somlyo, A., & Shao, Z. (1993a) *J. Microsc. 171*, 183−198.
Yang, J., Tamm, L., Tillack, T., & Shao, Z. (1993b) *J. Mol. Biol. 229*, 286−290.
Yang, J., Mou, J., & Shao, Z. (1994a) *Biochim. Biophys. Acta 1199*, 105−114.
Yang, J., Mou, J., & Shao, Z. (1994b) *FEBS Lett. 338*, 89−92.
Yu, J., Fischman, A., & Steck, T. (1973) *J. Supramol. Struct. 1*, 233−242.

BI9509816